The relationship between acoustic properties and the petrographic character of carbonate rocks

F. Rafavich, C. H. St. C. Kendall, and T. P. Todd

GEOPHYSICS, VOL. 49, NO. 10 (OCTOBER 1984); P. 1622-1636, 16 FIGS., 6 TABLES.

GEOPHYSICS, VOL. 49, NO. 10 (OCTOBER 1984); P. 1622-1636, 16 FIGS., 6 TABLES.

The relationship between acoustic properties and the petrographic character of carbonate rocks

F. Rafavich*, C. H. St. C. Kendall*, and T. P. Todd*

ABSTRACT

Laboratory studies of the detailed relationships between acoustic properties and the petrographic character of brine- and air-saturated carbonate rocks with a wide range of facies, porosities, lithologies, and rock fabrics indicate that porosity is the major factor influencing both *P*- and *S*-wave impedance and velocity. Primary lithology and secondary mineralogy have only a small influence on impedance and velocity. Combined use of *P*- and *S*-wave velocity data discriminates porosity changes from lithologic changes. All other variables, including pore-fluid type and petrographic fabric, have no significant influence on velocities.

Laboratory measurements of *P*-wave velocity under simulated in-situ conditions reproduce well-log velocity values reliably. Laboratory porosity-velocity trends agree with the time-average equation when the correct matrix velocities are used. Rock property results were used to interpret porosity/lithology variations for an inverted seismic section from the Williston basin. Where well control was available, the porosity/lithology interpretation was found to be in agreement with the subsurface control.

INTRODUCTION

Over recent years great interest has developed in shear waves. Now shear-wave velocity is available from well logging and seismic measurements. Laboratory and well-log studies (Pickett, 1963; Nations, 1974; Kithas, 1976; Gregory, 1977; Benzing, 1978; Johnson, 1978; Tatham, 1982; Eastwood, 1983) suggest a correlation between lithology, porosity, and V_p/V_s values. Theoretical work (Gardner and Harris, 1968; Kuster and Toksöz, 1974a, b) as well as laboratory data (King, 1966; Tatham and Stoffa, 1976; Gregory, 1976; Domenico, 1976) show the sensitivity of the V_p/V_s ratio to the pore fluid. This sensitivity explains the interest of explorationists in shear-wave velocity which can be a useful parameter for the analysis of rock properties in addition to compressional-wave velocity.

A laboratory investigation of the petrophysical characteristics of carbonate rocks was made to establish the relationship between compressional- and shear-wave velocity and the petrographic character of the carbonates. We chose an empirical approach to define and study these relationships. Because of the complexities inherent in the petrographic fabric of carbonate rocks, we chose not to model rock matrix velocities using existing theories (Voigt, 1928; Reuss, 1929; Gassman, 1951; Hill, 1952; Hashin and Shtrikman, 1962), but rather we used statistical techniques to try to identify complex, but systematic, relationships between compressional- and shear-wave velocities and the petrographic character of carbonate rocks. In many cases, however, models can be a useful and proper way to describe rock properties. We suggest that the empirical results of this study might be useful to other researchers to constrain such models in particular instances. We then use the statistical

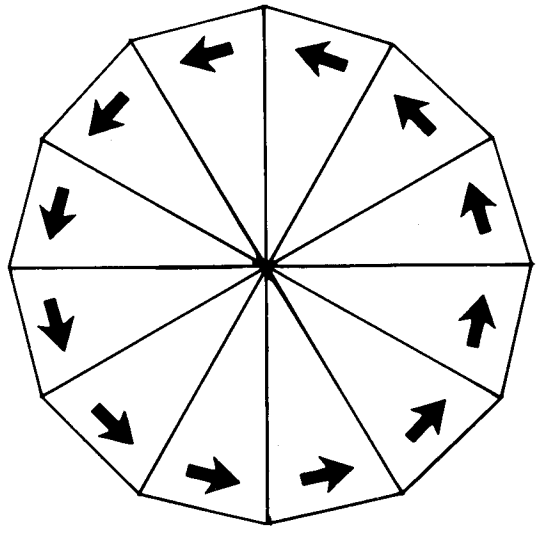

FIG. 1. Torsional shear-wave transducer.

Manuscript received by the Editor June 8, 1983; revised manuscript received April 27, 1984.
*Gulf Research and Development Company, P.O. Box 37048, Houston, TX 77099.

relationships so defined between the velocities and geologic parameters to interpret field velocity measurements. The second part of this paper presents an example of seismic-section interpretation using laboratory relationships between lithology, porosity, and impedance.

The rock samples used in this study came from four wells with cored sections in the Mission Canyon formation, Williston basin, North Dakota. The samples represent various carbonate facies (limestones, dolomites, anhydrites, and intermediate rock types). A total of 93 vertical plugs were cut from the cores to include as wide a variety of lithologies as possible.

The acoustic properties of rock samples were measured at differential pressures ranging from 500 to 10 000 psi. Although analysis of the data concentrated on the 6 000 psi differential pressure data, spot checks showed our results to be consistent with data taken over the entire range of pressure conditions.

Unless otherwise mentioned, the values for acoustic characteristics are for 6 000 psi differential pressure.

ACOUSTIC AND PETROPHYSICAL MEASUREMENTS

The *P*- and *S*-wave velocity measurements were made in a standard pressure cell under external pressures of 600 to 10 000 psi and constant internal pressure (100 psi) using the pulse transmission technique (Birch, 1960). The lead-zirconate/titanate transducers used for *P*- and *S*-wave velocity measurements had resonant frequency near 1 MHz. The transducer arrangement allowed the simultaneous measurement of *P*- and *S*-wave velocities under the same conditions.

The only unusual features of the equipment were "pie-shaped" *S*-wave transducers (Figure 1). These "torsional" transducers were manufactured by first cutting 12 pie-shaped slices of lead zirconate/titanate. These were glued together, with polarizations oriented to vibrate in a pure shear mode. The transducers enabled clean, high-amplitude shear-wave signals to be received.

The accuracy of the velocity measurements was about 1 percent for V_p and 2 percent for V_s. Sample porosity, density, and air permeability were made under room pressure using standard techniques. For each carbonate plug, an identification and subsurface depth were recorded, and the acoustic and petrophysical characteristics are presented in Table 1.

PETROGRAPHIC MEASUREMENTS

The petrographic and mineralogic data were determined from petrographic analysis of thin sections made from samples collected as close as possible to the corresponding carbonate plugs, and these were point counted (100 points per thin section) to determine the relative abundances of minerals, grains, muds, and crystals. The sizes of ten randomly chosen grains and crystals were also measured, and the mean and standard deviation for these two parameters were calculated. In addition, five major and minor axes of randomly selected pores were

Table 1. Measured acoustic and petrophysical characteristics.

	Original measurement	Symbolic name	Measurement unit
Brine-saturated samples	Confining pressure	—	psi
	porosity	PHI	percentage of total rock
	Permeability	KAY	mD
	Grain density	ROG	g/cm^3
	Bulk density	ROB	g/cm^3
	P-wave transit time	TPB	μs/ft
	S-wave transit time	TSB	μs/ft
Air-saturated samples	Bulk density	ROA	g/cm^3
	P-wave transit time	TPA	μs/ft
	S-wave transit time	TSA	μs/ft

In addition, values for the following parameter were derived from the acoustic data.

	Derived parameter	Symbolic name	Parameter unit
Brine-saturated samples	*P*-wave velocity (and impedance)	VPB (IPB)	ft/s (ft g/s cm^3)
	S-wave velocity (and impedance)	VSB (ISB)	ft/s (ft g/s cm^3)
	Ratio P/S wave velocity	VBR	dimensionless
Air-saturated samples	*P*-wave velocity (and impedance)	VPA (IPA)	ft/s (ft g/s cm^3)
	S-wave velocity (and impedance)	VSA (ISA)	ft/s (ft g/s cm^3)
	Ratio *P*/*S* wave velocity	VAR	dimensionless

Table 2. Petrographic measurements.

	Description	Symbolic name	Measurement unit
Grains	Oolite	OOG	Percentate of total rock
	Pisolite	PIG	Percentage of total rock
	Intraclast	ING	Percentage of total rock
	Pellet	PEG	Percentage of total rock
	Skeletal	SKG	Percentage of total rock
Mud	Calcite	CAM	Percentage of total rock
	Dolomite	DOM	Percentage of total rock
Crystals	Calcite	CAX	Percentage of total rock
	Dolomite	DOX	Percentage of total rock
	Anhydrite	ANX	Percentage of total rock
	Celestite	CEX	Percentage of total rock
	Quartz	QUX	Percentage of total rock
Composition	Calcite	CAC	Percentage of total rock
	Dolomite	DOC	Percentage of total rock
	Anhydrite	ANC	Percentage of total rock
	Celestite	CEC	Percentage of total rock
	Quartz	QUC	Percentage of total rock
Grain size	Mean	MUG	mm
	Std. dev.	SIG	mm
Crystal size	Mean	MUX	mm
	Std. dev.	SIX	mm
Pore size	Major axis	MXP	mm
	Minor axis	MNP	mm
	Ratio	RAT	Dimensionless
	Roundness	RND	Index from 0 to 1
Percentage	Grain	GTO	Percentage of total rock
	Crystal	XTO	Percentage of total rock
	Mud	MTO	Percentage of total rock
	Lithologic type	LIT	Code from 1 to 7

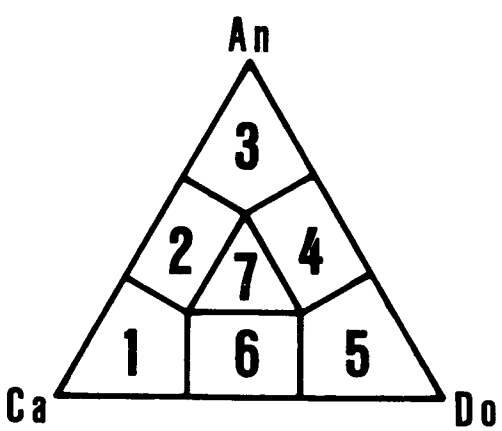

FIG. 2. The compositional terminology for rock types.

measured. The mineral composition of the thin sections was derived from modal analysis. Finally, the degrees of rounding, depositional setting, and lithologic rock types were estimated visually. A list of the recorded petrographic measurements is given in Table 2.

Seven lithologic groups were differentiated on the basis of mineral composition as exemplified in the triangular diagram of Figure 2. The end members are calcite, dolomite, and anhydrite; the lithology group cutoff points on all axes are 33 and 66 percent.

RESULTS

Graphical analysis

The original data, which are presented in Table 3, were analyzed statistically to ascertain the influence of the petrographic character of the rocks on the acoustic properties. The first step of the analysis was generation of crossplots to define major trends.

The relationship between *P*-wave velocity and porosity for brine-saturated samples can be approximated by the straight line shown in Figure 3. Values deduced from the time-average equations, calculated using grain velocities for pure calcite (21, 000 ft/s), dolomite (23 000 ft/s), anhydrite (20 000 ft/s), and brine (5 290 ft/s) are in good agreement with the laboratory data.

A clear velocity discrimination between carbonate rock types could not be obtained using only V_p versus porosity relationship (Figure 3). However, use of both *P*- and *S*-wave velocities in the form V_p/V_s versus V_p did favor limestone and dolomite discrimination. The crossplot of V_p/V_s versus V_p for brine-saturated samples is shown in Figure 4. The key to the lithologic codes is given in the inset. Rocks which are dominantly calcite (code 1) can clearly be separated from rocks which are dominantly dolomite (code 5). This coincides with the laboratory data of Pickett (1963) and Benzing (1978) and agrees well with the data derived from full-waveform sonic logs (Eastwood, 1983). With a lesser degree of certainty, anhydrites can be discriminated from the calcite and dolomite-rich rocks. Intermediate rock types have a strong overlap with the end members and, therefore, cannot be clearly distinguished.

Figure 5 shows that the distinction between limestones (code 1) and dolomites (code 5) can be established with velocities measured in air-saturated samples. Again, discrimination of anhydrites is less well established, and intermediate lithologic groups overlap with the end member groups. A comparison of Figures 4 and 5 shows that brine-saturated limestones and dolomites have higher V_p/V_s ratios than their air-saturated equivalents. The difference of the means, 5 to 6 percent, reflects the pore fluid.

The correlation coefficient between dolomite content and velocity is negative for V_p and not significantly different from zero for V_s for both brine- and air-saturated samples. A positive correlation was expected, since the mineral dolomite has a higher V_p than both calcite and anhydrite. However, Figure 3 shows that the dolomites in our sample suite are more porous than the limestones. The velocity decrease associated with porosity increase is stronger than the effect of increasing dolomite content, so the overall result is a decrease in *P*-wave velocity.

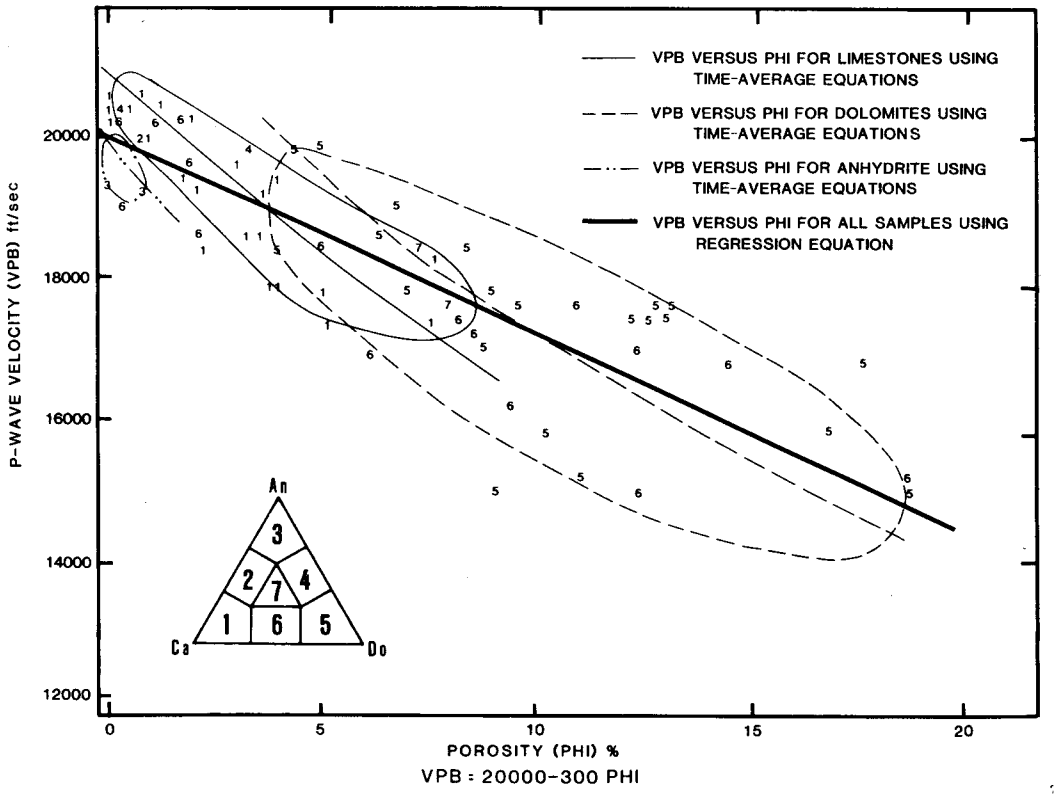

FIG. 3. Plot of *P*-wave velocities versus porosity for brine-saturated samples.

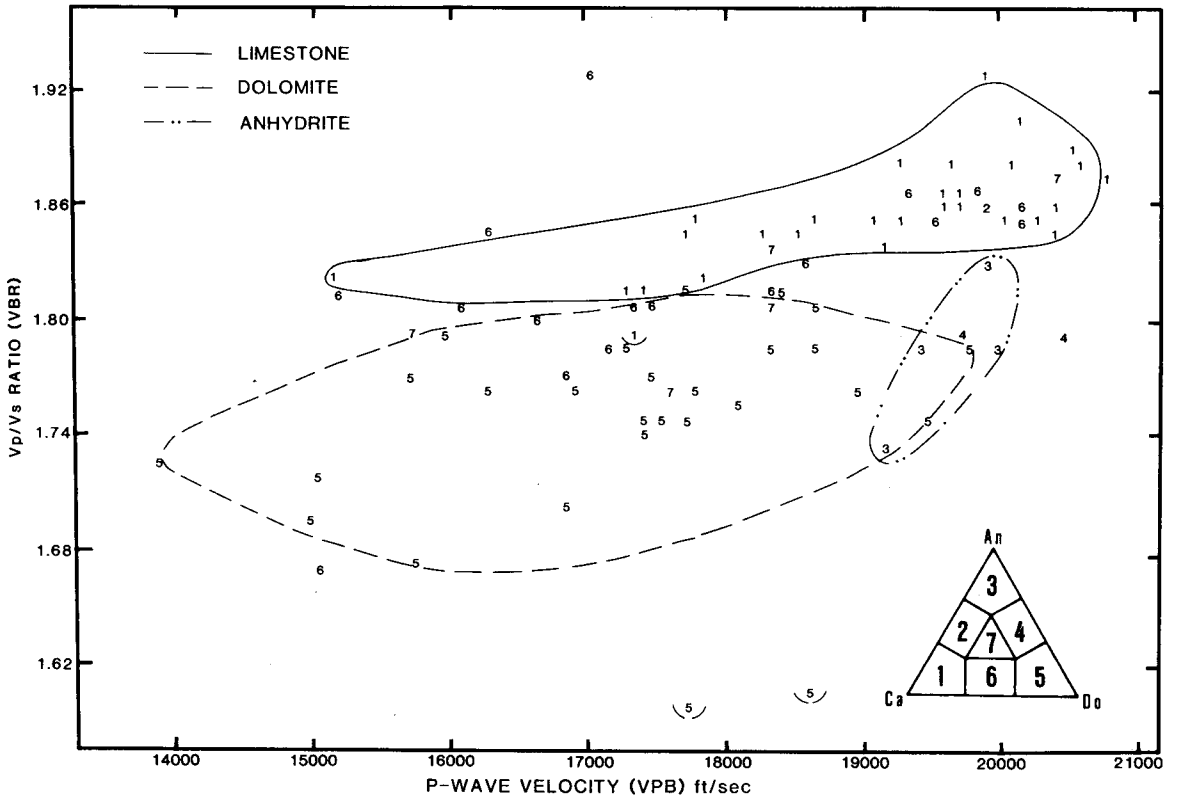

FIG. 4. Plot of V_p/V_s versus *P*-wave velocity for brine-saturated samples.

Table 3. Acoustic and petrographic data.

	DEPTH	KAY	LIT	PHI	ROG	ROB	RDA	DOG	PIG	ING	PEG	SKG	CAM	DOM	CAX	DOX	ANX	CEX	QUX	CAC	DOC
WELL 1	3996.5	0.0100	3	0.710	2.930	2.920	2.910	0	0	0	0	0	0	0	0	15	85	0	0	0	15
	3997.0	0.0001	5	8.900	2.730	2.570	2.490	0	0	0	0	0	0	0	0	53	15	0	23	0	53
	4009.0	0.0100	5	17.400	2.820	2.500	2.330	0	0	0	0	0	0	0	0	82	0	0	1	0	82
	4010.5	0.0900	5	18.600	2.810	2.470	2.290	0	0	0	0	0	0	0	11	69	0	0	1	11	69
	4011.5	0.0100	1	1.350	2.750	2.730	2.710	0	0	0	0	0	91	0	0	0	8	0	0	91	0
	4013.5	1.1000	5	13.000	2.800	2.570	2.440	0	0	0	0	0	0	66	17	0	4	0	0	17	66
	4015.5	0.0001	1	3.570	2.760	2.700	2.660	0	32	5	0	0	42	0	3	0	14	0	0	82	0
	4016.0	0.0001	1	3.630	2.720	2.650	2.620	59	1	12	1	0	10	0	2	0	11	0	0	85	0
	4017.5	0.0001	1	3.140	2.700	2.650	2.620	27	5	31	3	0	0	0	29	2	0	0	0	90	7
	4020.0	0.0001	1	7.710	2.700	2.570	2.490	0	0	0	1	4	70	0	17	0	0	0	0	92	0
	4024.0	0.0100	7	7.390	2.720	2.600	2.520	2	12	3	19	1	27	7	1	1	20	0	0	53	20
	4027.0	0.0100	6	13.500	2.710	2.480	2.340	0	0	0	0	8	27	38	3	10	0	0	0	38	48
	4029.0	0.0001	6	6.120	2.680	2.580	2.520	0	0	0	0	9	10	0	37	38	0	0	0	56	38
	4033.0	0.0100	6	11.000	2.770	2.580	2.470	0	0	0	0	0	47	42	0	0	0	0	0	47	42
	4035.0	6.3000	1	17.100	2.720	2.430	2.250	30	13	6	8	0	0	0	21	5	0	0	0	65	18
	4035.8	0.0300	7	7.700	2.790	2.650	2.580	25	12	6	8	0	9	3	0	3	26	0	0	48	18
	4036.0	0.0001	5	6.480	2.940	2.810	2.750	57	11	11	1	1	0	1	0	12	0	0	0	21	73
	4037.0	0.0100	6	12.700	2.750	2.530	2.400	61	0	1	0	1	5	14	0	4	1	0	0	35	52
	4041.0	0.0100	6	8.520	2.720	2.580	2.490	0	0	21	0	0	0	0	23	47	0	0	0	44	47
	4042.0	0.0400	5	13.400	2.790	2.550	2.420	0	3	18	0	2	0	64	0	0	0	0	0	8	79
	4042.5	0.7900	6	12.300	2.740	2.530	2.400	0	19	48	0	0	1	9	0	11	0	0	0	48	34
	4043.5	2.4000	7	15.100	2.960	2.660	2.510	0	4	8	7	0	9	5	7	11	34	0	0	31	20
	4044.0	6.9000	6	18.700	2.740	2.530	2.230	0	16	4	14	5	0.	0	7	35	0	0	0	30	51
	4045.0	7.2000	6	14.300	2.780	2.520	2.380	0	0	0	6	0	24	51	0	0	1	0	4	30	51
	4047.0	0.4700	4	3.400	2.850	2.790	2.750	0	0	0	0	0	9	4	7	27	50	0	0	16	31
	4049.0	0.0100	7	2.130	3.170	3.130	3.100	0	0	0	0	0	0	0	17	15	36	30	0	17	15
	4050.0	0.0200	3	0.010	2.930	2.930	2.930	0	0	0	0	0	0	0	0	0	100	0	0	0	0
	4052.5	0.0001	3	0.010	2.920	2.920	2.920	0	0	0	0	0	0	0	0	0	100	0	0	0	0
WELL 2	9766.5	0.0001	1	0.716	2.715	2.703	2.696	0	0	62	0	4	0	0	14	7	6	0	0	86	7
	9780.5	0.0001	1	4.043	2.737	2.667	2.626	0	0	31	13	0	0	0	24	27	1	0	0	68	27
	9787.5	0.0100	1	3.335	2.684	2.629	2.594	0	4	58	10	1	0	0	23	1	0	0	0	96	1
	9794.5	0.0100	1	2.068	2.703	2.668	2.647	0	2	84	0	0	0	0	12	0	0	0	0	98	0
	9810.5	0.0001	6	1.775	2.748	2.717	2.699	0	0	15	0	7	0	0	30	45	1	0	0	52	45
	9834.5	0.0100	5	6.874	2.760	2.640	2.570	0	0	0	0	0	0	0	7	83	3	0	0	7	83
	9843.5	0.0100	6	5.030	2.739	2.652	2.601	0	0	2	0	1	0	0	40	52	0	0	0	41	54
	9849.5	0.0001	5	9.038	2.790	2.630	2.538	0	0	0	0	1	0	74	12	1	0	0	3	13	75
	9856.5	0.0001	5	6.752	2.829	2.707	2.638	0	0	0	0	0	0	0	0	93	0	0	0	0	93
	9865.5	0.0001	5	5.240	2.778	2.685	2.532	0	0	0	0	22	0	0	10	63	0	0	0	32	63
	9877.5	0.0001	5	4.365	3.197	3.101	3.056	0	0	0	0	0	0	0	2	92	0	2	0	2	92
	9889.5	0.0001	6	2.254	2.697	2.659	2.636	0	0	0	0	29	0	0	43	24	2	0	0	60	36
	9897.5	0.0001	5	6.894	2.811	2.687	2.617	0	0	0	0	0	0	0	1	92	0	0	0	1	92
	9931.5	0.3100	5	13.143	2.819	2.582	2.448	0	0	0	0	0	0	0	7	80	0	0	0	7	80
	9935.5	0.0001	6	1.656	2.714	2.686	2.669	0	0	0	0	19	0	0	29	50	0	0	0	36	62
	9939.5	0.0001	5	7.080	2.795	2.670	2.598	0	0	0	0	0	0	0	7	85	1	0	0	7	85
	9944.5	0.0001	6	1.239	2.748	2.727	2.714	0	0	0	0	36	0	0	0	63	0	0	0	36	63
WELL 3	10032.5	0.0100	5	8.449	2.705	2.562	2.476	0	0	0	0	0	0	0	0	87	1	4	0	0	87
	10076.5	0.0001	1	3.149	2.694	2.641	2.609	0	0	0	0	58	0	0	37	2	0	0	0	95	2
	10099.5	0.1500	5	12.752	2.829	2.597	2.468	0	0	0	0	2	0	0	23	62	0	0	0	25	62
	10123.5	0.0001	6	1.932	2.722	2.689	2.669	0	0	0	0	34	0	0	30	34	0	0	0	64	34
	10134.5	0.0001	6	1.300	2.709	2.687	2.674	0	0	0	0	49	0	0	15	35	0	0	0	64	35
	10167.5	0.0001	1	3.558	2.715	2.654	2.618	0	0	0	0	20	0	0	54	22	0	0	0	74	22
	10178.5	0.0001	1	0.603	2.713	2.703	2.697	0	0	0	0	41	0	0	36	19	0	3	0	77	19
	9968.5	5.0000	5	16.774	2.771	2.476	2.306	0	0	0	0	0	0	0	0	78	1	4	0	0	78
	9983.5	0.2500	6	12.382	2.702	2.493	2.367	0	0	0	8	0	3	0	17	46	0	4	0	28	46
	10045.5	0.3600	1	7.417	2.674	2.551	2.476	0	0	0	0	89	0	0	4	0	0	0	0	93	0
	10084.5	1.0000	6	8.263	2.720	2.579	2.495	0	0	0	0	47	0	0	11	34	0	0	0	58	34
WELL 4	9692.6	0.0001	5	10.266	2.788	2.606	2.502	0	0	0	0	0	0	0	0	88	0	0	2	0	88
	9706.0	0.0100	4	0.300	2.911	2.911	2.902	0	0	0	0	0	0	0	0	40	60	0	0	0	40
	9732.5	0.0100	3	0.200	2.944	2.944	2.938	0	0	0	0	0	0	0	0	19	81	0	0	0	19
	9736.7	0.0001	2	0.856	2.766	2.751	2.742	0	0	0	0	7	42	0	10	15	25	0	0	59	15
	9760.0	0.0100	7	0.388	2.828	2.821	2.817	0	8	23	0	0	0	0	0	19	50	0	0	31	19
	9778.6	0.0001	1	0.248	2.695	2.691	2.688	0	0	0	0	17	26	0	57	0	0	0	0	100	0
	9794.0	0.4300	6	9.348	2.720	2.560	2.711	0	1	6	0	2	41	0	0	32	4	0	0	55	32
	9801.6	0.4000	5	17.553	2.824	2.506	2.328	0	0	0	0	0	0	0	0	80	0	0	2	0	80
	9815.6	0.0100	5	8.871	2.730	2.578	2.488	0	0	0	0	0	0	0	0	91	0	0	0	0	91
	9820.6	--	-	8.323	2.677	2.538	2.454	-	-	-	-	-	-	-	-	-	-	-	-	-	-
	9825.8	1.0000	5	12.255	2.828	2.606	2.481	0	0	0	0	0	0	0	0	88	0	0	0	0	88
	9837.0	0.0001	5	5.066	2.807	2.718	2.665	0	0	0	0	0	0	0	0	95	0	0	0	0	95
	9852.0	3.9000	5	3.917	2.714	2.647	2.608	0	0	0	0	0	0	0	8	88	0	0	0	8	88
	9858.0	0.0100	5	6.043	2.721	2.618	2.557	0	0	0	0	0	0	0	4	90	0	0	0	4	90
	9894.0	0.0001	5	9.682	2.800	2.627	2.529	0	0	0	0	0	0	0	4	86	0	0	0	4	86
	9906.4	0.0001	6	1.068	2.721	2.703	2.692	0	0	0	0	28	4	0	8	53	2	0	4	40	53
	9938.0	0.0100	5	11.046	2.671	2.488	2.376	0	0	0	0	9	0	0	0	67	1	0	12	9	67
	9951.8	0.1000	5	8.425	2.806	2.655	2.570	0	0	0	0	0	0	0	17	75	0	0	0	17	75
	9964.0	0.4300	5	10.663	2.751	2.566	2.458	0	0	0	0	15	0	0	6	68	0	0	0	21	68
	9969.0	0.0001	1	1.290	2.687	2.665	2.652	0	0	0	0	60	31	0	5	0	3	0	0	96	0
	10005.0	0.0001	1	0.984	2.695	2.679	2.668	0	0	0	0	49	50	0	0	0	0	0	0	99	0
	10037.6	0.0100	5	12.533	2.829	2.601	2.474	0	0	0	0	0	0	0	0	87	0	0	0	0	87
	10047.8	1.1000	1	8.696	2.737	2.587	2.499	0	0	0	0	0	0	0	68	23	0	0	0	68	23
	10062.6	0.0100	1	4.987	2.706	2.622	2.571	0	0	0	0	28	25	0	28	14	0	0	0	81	14
	10067.6	0.0001	1	4.239	2.726	2.654	2.610	0	0	0	0	21	0	0	51	24	0	0	0	72	24
	10094.0	0.0001	1	3.955	2.703	2.636	2.596	0	0	0	0	44	26	0	0	26	0	0	0	70	26
	10112.4	0.0001	1	2.473	2.699	2.658	2.632	0	0	6	21	38	29	0	4	0	0	0	0	98	0
	8862.0	0.0001	1	0.147	2.693	2.690	2.689	0	0	40	0	5	44	8	3	0	0	0	0	92	8
	8869.0	0.0001	5	2.118	2.643	2.609	2.587	0	0	0	0	0	8	58	4	28	0	0	0	12	86
	8877.0	0.0001	1	5.247	2.684	2.596	2.543	0	0	0	0	6	50	4	16	17	0	0	0	74	21
	8907.0	0.0001	1	1.113	2.699	2.680	2.669	0	0	0	0	13	29	7	28	22	0	0	0	70	29
	8956.0	0.0001	6	0.474	2.691	2.683	2.678	0	0	0	0	26	26	18	28	0	0	0	2	54	44
	8984.0	0.0001	6	0.449	2.698	2.691	2.686	0	0	0	0	24	0	18	40	18	0	0	0	64	36
	9003.0	0.0001	1	0.272	2.673	2.669	2.666	0	0	0	0	43	14	0	43	0	0	0	0	100	0
	9014.5	0.0001	1	2.295	2.678	2.640	2.617	0	0	0	0	38	8	0	50	2	0	0	0	96	2
	9041.0	0.0001	1	0.229	2.696	2.693	2.690	0	0	0	0	16	28	0	32	24	0	0	0	76	24
	9088.0	0.0001	1	0.754	2.687	2.675	2.667	0	0	0	0	28	60	0	10	1	0	0	0	98	1

Table 3. (Continued)

ANC	CEC	QUC	MUG	SIG	MUX	SIX	NXP	MNP	RAT	RND	GTO	MTO	XTO	VPB	VSB	VPA	VSA
85	0	0	0.00	0.00	0.07	0.06	0.00	0.00	0.00	0.0	0	0	100	19193.9	11061.9	19157.1	11198.2
15	0	23	0.00	0.00	0.03	0.02	0.00	0.00	0.00	0.2	0	0	91	15015.0	8849.6	14771.0	9523.8
0	0	1	0.00	0.00	0.02	0.01	0.08	0.05	1.60	0.0	0	0	83	13927.6	8064.5	14450.9	9259.3
0	0	1	0.00	0.00	0.07	0.06	0.00	0.00	0.00	0.0	0	0	81	15083.0	8771.9	15408.3	9523.8
8	0	0	0.00	0.00	0.00	0.00	0.00	0.00	0.00	0.0	0	91	8	20408.2	10952.9	19920.3	11001.1
4	0	0	1.43	1.29	0.09	0.11	0.13	0.07	1.86	0.1	0	66	21	17301.0	9708.7	17035.8	10080.6
14	0	0	0.98	0.72	0.45	0.22	0.11	0.07	1.57	0.8	37	42	17	19762.8	10627.0	19084.0	10672.4
11	0	0	0.86	0.70	0.39	0.21	0.25	0.11	2.27	0.8	72	10	13	19157.1	10427.5	18518.5	10482.2
0	0	0	0.75	0.67	0.06	0.14	0.15	0.12	1.25	0.8	66	0	31	19685.0	10471.2	19379.8	10582.0
0	0	0	0.00	0.00	0.04	0.03	0.07	0.05	1.40	0.8	5	70	17	18281.5	9901.0	17825.3	10090.8
20	0	0	0.59	0.41	0.20	0.25	0.19	0.13	1.46	0.8	37	34	22	18382.4	10000.0	17857.1	10101.0
0	0	0	0.25	0.28	0.01	0.01	0.06	0.05	1.20	0.1	8	65	13	16339.9	8849.6	16025.6	9090.9
0	0	0	0.20	0.09	0.00	0.00	0.00	0.00	0.00	0.8	9	10	75	16891.9	9523.8	16447.4	9615.4
0	0	0	0.00	0.00	0.02	0.02	0.07	0.04	1.75	0.0	0	89	0	17513.1	9708.7	17513.1	10060.4
0	0	0	0.48	0.20	0.01	0.01	0.10	0.09	1.11	0.9	57	0	26	15197.6	8333.3	15060.2	8849.6
26	0	0	0.67	0.58	0.11	0.17	0.12	0.11	1.09	1.0	51	12	29	17605.6	10000.0	17543.9	10245.9
0	0	0	0.55	0.59	0.01	0.01	0.11	0.08	1.38	0.9	81	1	12	18691.6	10460.3	18281.5	10593.2
0	0	0	0.41	0.15	0.02	0.01	0.11	0.10	1.10	0.8	63	19	5	16666.7	9259.3	16611.3	9615.4
0	0	0	1.07	0.63	0.08	0.05	0.10	0.07	1.43	0.5	21	0	70	17182.1	9615.4	16863.4	9803.9
0	0	0	0.56	0.73	0.00	0.00	0.10	0.08	1.25	0.3	23	64	0	16339.9	9259.3	16103.1	9803.9
6	0	0	0.48	0.28	0.02	0.01	0.16	0.12	1.33	0.5	67	10	11	17064.8	8849.6	16666.7	9174.3
34	0	0	0.36	0.31	0.04	0.09	0.15	0.10	1.50	0.7	19	14	52	15748.0	8771.9	15503.9	8695.7
0	0	0	0.44	0.36	0.01	0.01	0.11	0.08	1.38	1.0	39	0	42	15220.7	8403.4	14992.5	8928.6
1	0	4	0.22	0.13	0.03	0.02	0.03	0.02	1.25	0.5	6	75	5	16806.7	9901.0	16694.5	10193.7
50	0	0	0.00	0.00	0.00	0.00	0.03	0.03	1.00	0.5	0	13	84	19762.8	11037.5	19723.9	11185.7
36	30	0	0.00	0.00	0.22	0.22	0.00	0.00	0.00	0.0	0	0	98	18382.4	10172.9	17857.1	10245.9
100	0	0	0.00	0.00	0.03	0.03	0.00	0.00	0.00	0.0	0	0	100	19455.3	10917.0	19607.8	11299.4
100	0	0	0.00	0.00	0.00	0.00	0.00	0.00	0.00	0.0	0	0	100	20000.0	11198.2	19685.0	11198.2
6	0	0	0.22	0.16	0.29	0.27	0.18	0.17	1.06	0.5	72	0	27	20618.6	10940.9	19455.3	10846.0
1	0	0	0.59	0.96	0.03	0.03	0.19	0.18	1.06	0.8	44	0	52	19305.0	10416.7	18518.5	10615.7
0	0	0	0.63	0.45	0.25	0.17	0.21	0.18	1.17	0.7	73	0	24	19723.9	10582.0	19157.1	10661.0
0	0	0	0.83	1.01	0.27	0.35	0.26	0.15	1.73	0.0	86	0	12	20120.7	10695.2	19920.3	10741.1
1	0	0	0.49	0.62	0.05	0.03	0.19	0.16	1.19	0.0	22	0	76	20242.9	10729.6	18348.6	10741.1
3	0	0	0.00	0.00	0.04	0.02	0.08	0.03	2.67	0.0	0	0	93	18115.9	10319.9	16366.6	10266.9
0	0	0	0.20	0.15	0.04	0.01	0.03	0.03	1.00	0.0	3	0	92	18382.4	10142.0	17006.8	10224.9
0	0	0	0.23	0.07	0.01	0.01	0.05	0.04	1.25	0.0	1	74	16	17793.6	10101.0	17482.5	10604.5
0	0	0	0.00	0.00	0.08	0.12	0.03	0.03	1.00	0.0	0	0	93	19493.2	11173.2	19802.0	11507.5
0	0	0	0.95	1.82	0.02	0.01	0.05	0.03	1.67	0.5	22	0	73	18691.6	10330.6	17699.1	10559.7
0	2	0	0.00	0.00	0.01	0.00	0.05	0.03	1.67	0.0	0	0	96	19723.9	11025.4	18348.6	11325.0
2	0	0	0.38	0.54	0.02	0.01	0.09	0.07	1.29	0.4	29	0	69	18622.0	10193.7	17605.6	10277.5
0	0	0	0.00	0.00	0.01	0.01	0.00	0.00	0.00	0.0	0	0	93	18975.3	10752.7	18083.2	11037.5
0	0	0	0.00	0.00	0.03	0.05	0.00	0.00	0.00	0.0	0	0	87	17543.9	10040.2	17985.6	10526.3
0	0	0	0.70	0.73	0.02	0.01	0.11	0.09	1.27	0.0	19	0	79	19379.8	10384.2	18382.4	10787.5
1	0	0	0.00	0.00	0.01	0.00	0.07	0.03	2.33	0.0	0	0	93	17730.5	10142.0	15923.6	10266.9
0	0	0	0.77	0.91	0.02	0.01	0.00	0.00	0.00	0.5	36	0	63	20202.0	10893.2	18975.3	11037.5
1	4	0	0.00	0.00	0.01	0.01	0.03	0.02	1.50	0.0	0	0	92	17730.5	11098.8	17605.6	11350.7
0	0	0	1.04	0.71	0.11	0.10	0.34	0.14	2.43	0.0	58	0	39	18656.7	10090.8	16977.9	10030.1
0	0	0	0.34	0.17	0.04	0.04	0.00	0.00	0.00	0.0	2	0	85	17636.7	10000.0	17331.0	10362.7
0	0	0	0.37	0.32	0.02	0.01	0.04	0.03	1.33	0.0	34	0	64	19531.3	10562.3	18587.4	10672.4
0	0	0	0.37	0.30	0.04	0.05	0.00	0.00	0.00	0.5	49	0	50	19880.7	10649.6	18939.4	10661.0
0	0	0	0.27	0.23	0.02	0.01	0.04	0.04	1.00	0.5	20	0	76	18587.4	10090.8	18050.5	10395.0
0	3	0	0.35	0.27	0.01	0.00	0.04	0.03	1.33	0.6	41	0	58	20449.9	11061.9	20000.0	11098.8
1	4	0	0.00	0.00	0.02	0.01	0.12	0.08	1.50	0.0	0	0	83	15748.0	9434.0	15822.8	9901.0
0	14	0	0.33	0.21	0.02	0.01	0.10	0.07	1.51	0.0	11	0	67	15037.6	9009.0	14881.0	9523.8
0	0	0	0.44	0.24	0.23	0.08	0.41	0.20	2.05	0.0	89	0	4	17301.0	9523.8	16583.7	9615.4
0	0	0	1.03	0.88	0.02	0.01	0.05	0.03	1.57	0.4	47	0	45	17391.3	9615.4	16920.5	9901.0
0	0	2	0.00	0.00	0.01	0.01	0.00	0.00	0.00	0.0	0	0	90	15772.9	8928.6	15384.6	9615.4
60	0	0	0.00	0.00	0.01	0.01	0.00	0.00	0.00	0.0	0	0	100	20491.8	11441.6	20790.0	11560.7
81	0	0	0.00	0.00	0.00	0.00	0.00	0.00	0.00	0.0	0	0	100	19920.3	10905.1	19960.1	10869.6
25	0	0	0.34	0.41	0.71	1.18	0.00	0.00	0.00	0.0	7	42	50	19960.1	10729.6	18315.0	10649.6
50	0	0	0.38	0.32	0.04	0.03	0.00	0.00	0.00	0.0	31	0	69	20449.9	10893.2	18587.4	10752.7
0	0	0	0.16	0.09	0.03	0.02	0.00	0.00	0.00	0.0	17	26	57	20833.3	11111.1	20876.8	11111.1
4	0	0	0.37	0.21	0.12	0.15	0.14	0.08	1.68	0.0	9	41	36	16129.0	8928.6	15949.0	9009.0
0	0	2	0.00	0.00	0.03	0.01	0.04	0.04	1.11	0.0	0	0	82	16863.4	9901.0	17064.8	10288.1
0	0	0	0.00	0.00	0.02	0.02	0.04	0.03	1.50	0.0	0	0	91	16920.5	9615.4	17182.1	10298.7
-	-	-	-	-	-	-	-	-	-	-	-	-	-	16233.8	9434.0	16286.6	9001.0
0	0	0	0.00	0.00	0.03	0.01	0.13	0.09	1.49	0.0	0	0	88	17452.0	10040.2	17452.0	10449.3
0	0	0	0.00	0.00	0.02	0.02	0.02	0.01	1.77	0.0	0	0	95	19802.0	11111.1	20000.0	11534.0
0	0	0	0.00	0.00	0.01	0.01	0.00	0.00	0.00	0.0	0	0	96	18450.2	10183.3	17605.6	10352.0
0	0	0	0.00	0.00	0.04	0.05	0.09	0.05	1.62	0.0	0	0	94	17762.0	9803.9	17123.3	10000.0
0	0	0	0.00	0.00	0.01	0.00	0.03	0.02	2.00	0.0	0	0	90	17513.1	9901.0	17543.9	10504.2
2	0	4	0.28	0.46	0.07	0.19	0.00	0.00	0.00	0.0	28	0	67	19723.9	10615.7	18214.9	10718.1
1	0	12	0.36	0.32	0.02	0.01	0.00	0.00	0.00	0.0	9	0	80	15243.9	9009.0	14705.9	9434.0
0	0	0	0.00	0.00	0.02	0.01	0.00	0.00	0.00	0.0	0	0	92	18382.4	10319.9	18518.5	10752.7
0	0	0	0.23	0.18	0.01	0.01	0.05	0.03	1.35	0.1	15	0	74	16025.6	8928.6	16207.5	9523.8
3	0	0	0.14	0.12	0.02	0.02	0.00	0.00	0.00	0.5	60	31	8	19607.8	10548.5	18691.6	10548.5
0	0	0	0.36	0.34	0.00	0.00	0.00	0.00	0.00	0.5	49	50	0	20040.1	10799.1	18797.0	10695.2
0	0	0	0.00	0.00	0.01	0.01	0.22	0.16	1.40	0.0	0	0	87	17452.0	10000.0	17667.8	10504.2
0	0	0	1.26	1.32	0.09	0.13	0.20	0.10	1.87	0.0	0	0	91	17391.3	9708.7	17605.6	10000.0
0	0	0	0.66	1.15	0.03	0.01	0.00	0.00	0.00	0.5	28	25	42	17421.6	9615.4	17035.8	9901.0
0	0	0	0.36	0.31	0.03	0.02	0.00	0.00	0.00	0.2	21	0	75	17762.0	9615.4	16556.3	9803.9
0	0	0	0.41	0.55	0.02	0.01	0.00	0.00	0.00	0.5	44	26	26	17825.3	9615.4	16611.3	9803.9
0	0	0	0.15	0.12	0.00	0.00	0.00	0.00	0.00	0.5	65	29	4	19342.4	10266.9	18832.4	10482.2
0	0	0	0.00	0.00	0.02	0.01	0.00	0.00	0.00	0.0	45	52	3	20325.2	10964.9	20833.3	11198.2
0	0	0	0.00	0.00	0.03	0.01	0.00	0.00	0.00	0.0	0	66	32	18622.0	11587.5	18484.3	11820.3
0	0	0	0.11	0.05	0.04	0.05	0.05	0.04	1.19	0.0	8	54	33	17889.1	9803.9	17921.1	10000.0
0	0	0	0.52	0.57	0.06	0.06	0.00	0.00	0.00	0.0	13	36	50	19646.4	10537.4	19417.5	10683.8
0	0	2	1.12	1.11	0.01	0.01	0.00	0.00	0.00	0.5	26	44	30	20161.3	10822.5	19607.8	10917.0
0	0	0	0.04	0.52	0.03	0.02	0.00	0.00	0.00	0.0	24	18	58	19011.4	9901.0	19723.9	10672.4
0	0	0	0.65	0.76	0.02	0.01	0.00	0.00	0.00	0.0	43	14	43	20161.3	10582.0	19191.9	10649.6
0	0	0	1.43	1.79	0.10	0.18	0.00	0.00	0.00	0.0	38	8	52	19120.5	10309.3	18622.0	10449.3
0	0	0	0.30	0.28	0.02	0.02	0.00	0.00	0.00	0.0	16	28	56	20533.9	10857.8	20242.9	10976.9
0	0	0	0.33	0.18	0.07	0.02	0.00	0.00	0.00	0.0	28	60	11	19920.3	10352.0	18797.0	10582.0

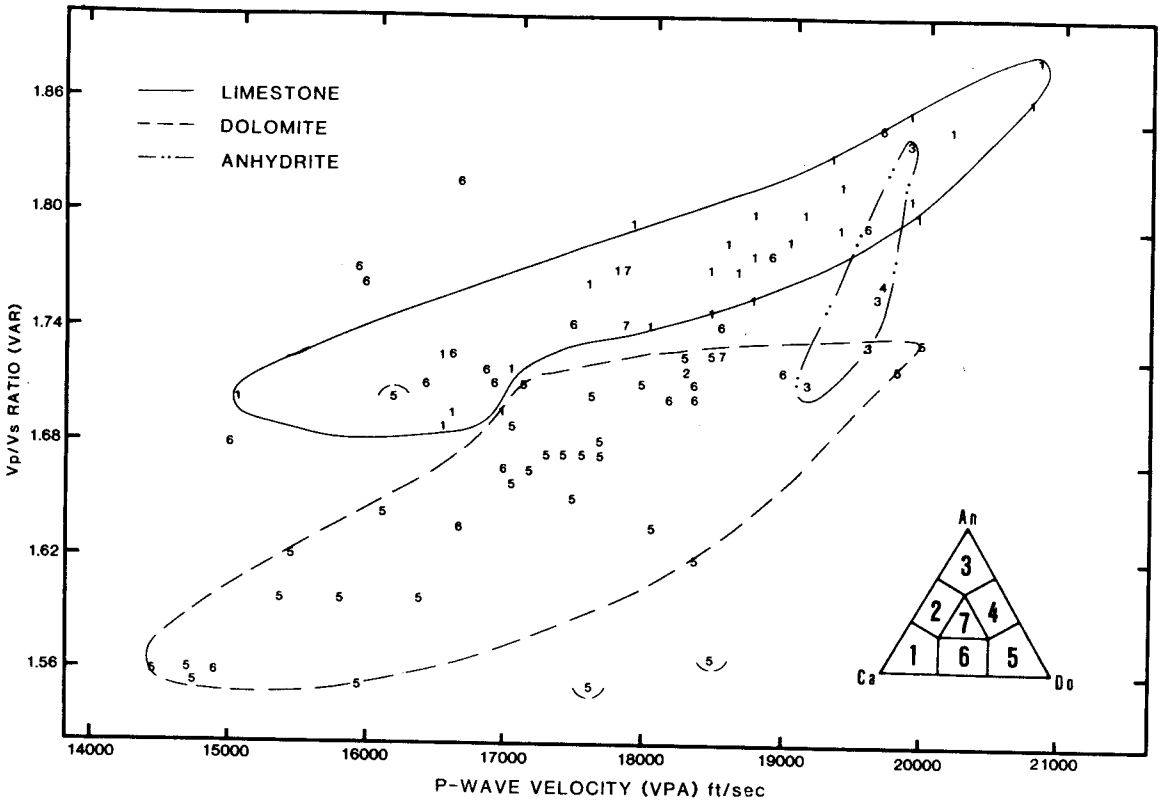

FIG. 5. Plot of V_p/V_s versus P-wave velocity for air-saturated samples.

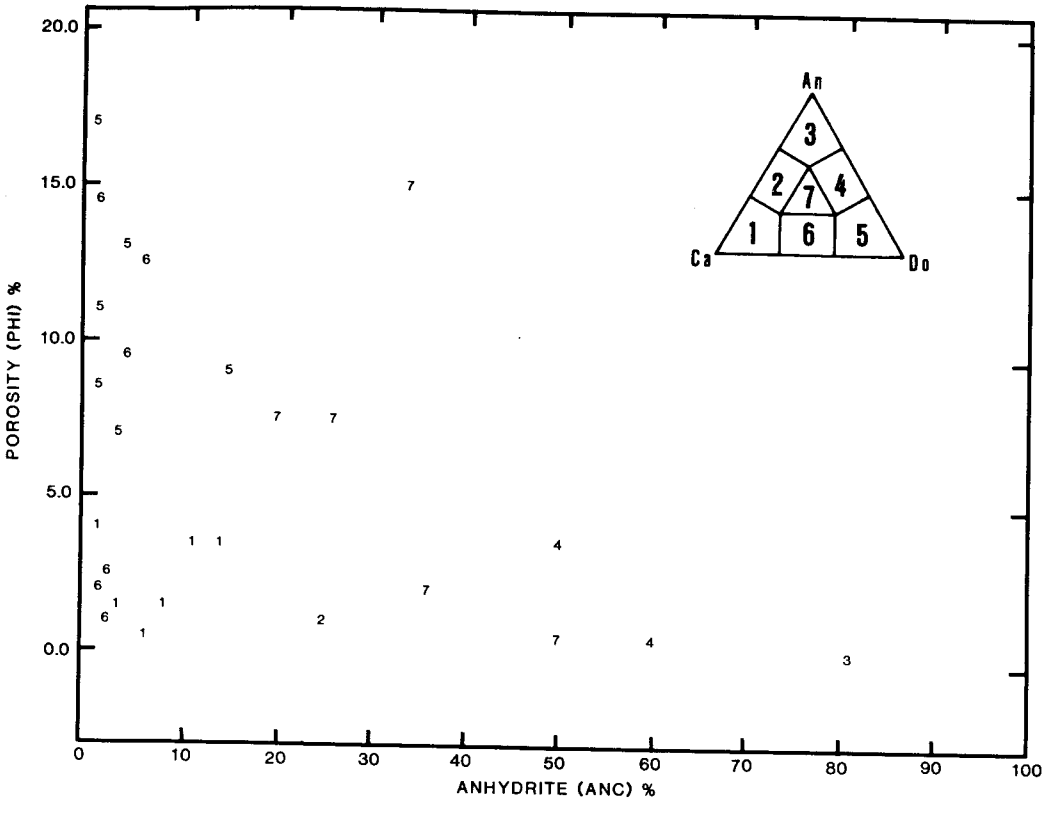

FIG. 6. Plot of porosity versus anhydrite content.

Table 4. Coefficients for the independent variables.

Differential pressure (psi)	A_0	A_1	A_2	A_3	A_4	A_5	A_6	A_7	A_8
				VPB					
500	−3 550	8 450	200	90	13	11	10	5	5
2 000	−750	7 450	180	80	15	0	0	4	3
4 000	950	6 950	160	80	16	0	0	3	2
6 000	1 550	6 800	160	80	18	0	0	2	2
8 000	2 150	6 600	150	80	19	0	0	1	1
10 000	2 250	6 550	150	80	20	0	0	0	0
				VPA					
500	6 300	4 600	140	140	0	33	30	5	4
2 000	8 150	3 950	120	120	0	20	18	4	3
4 000	8 650	3 900	120	120	0	14	12	2	2
6 000	8 800	3 900	120	110	0	9	9	2	1
8 000	8 650	4 050	130	110	10	8	7	0	0
10 000	8 350	4 150	130	110	11	0	0	0	0
				VSB					
500	−750	4 050	100	0	0	11	10	2	2
2 000	1 050	3 500	80	0	0	7	7	1	1
4 000	2 050	3 250	80	34	7	6	5	0	0
6 000	2 500	3 100	70	34	7	5	4	0	0
8 000	2 850	3 000	70	34	8	4	4	0	0
10 000	2 900	2 950	70	33	8	0	0	0	0
				VSA					
500	4 900	2 150	70	0	0	15	14	0	0
2 000	5 550	1 950	60	0	0	10	9	0	0
4 000	6 050	1 850	60	32	6	7	7	0	0
6 000	6 150	1 800	60	31	6	6	5	−1	−1
8 000	6 150	1 850	60	28	7	5	5	−1	−1
10 000	6 150	1 900	60	29	8	5	4	−1	−1

For *S*-wave velocities, the dolomite and porosity effects seem to offset each other.

The presence of anhydrite usually tends to decrease the rock porosity (Figure 6) and increase the velocities. In rocks composed mainly of dolomite and anhydrite, porosity values can be low and matrix velocity values high. Consequently, the velocities in such rocks might be higher than in pure anhydrite.

Statistical relationships

To obtain mathematical relationships between *P*- and *S*-wave velocities and the petrographic characteristics of Table 2, we used multiple regression analysis. However, classical methods of multiple linear regression (Bryant, 1960) did not resolve our problem satisfactorily, presumably because of strong correlations between some variables. Standard factor analysis (Harman, 1976) which allows the computation of a set of principal components, followed by the computation of the regression on principal component scores, did not work either, because of the complex nature of our data. Unrotated principal components show significant loadings attributable to a large number of variables. Therefore, a special technique of multiple regression was adopted which involved a regression analysis performed on factor scores from individually computed and rotated factorial axes. The response variable is velocity; the regressors are the factor scores computed using only the observed petrographic data. First, rotated principal components were calculated to maximize the principal component loading of several variables on each axis, while keeping all other loadings small. Then each principal component was recalculated using only the original variables which showed high loadings on this axis. The purpose is to eliminate entirely the small loadings which were still present and maintain some degree of correlation between the axes. After that, regression on the principal component scores was computed.

The advantages of this method are that it utilizes all the information available in the data matrix and removes all correlations between axes prior to the multiple regression. Also, since principal component and regression analyses both involve linear transformations of the input data, we can readily restore the relationship between the independent variable (velocity) and original predictor variables.

The regression equations for V_p and V_s were derived using this multiple regression technique:

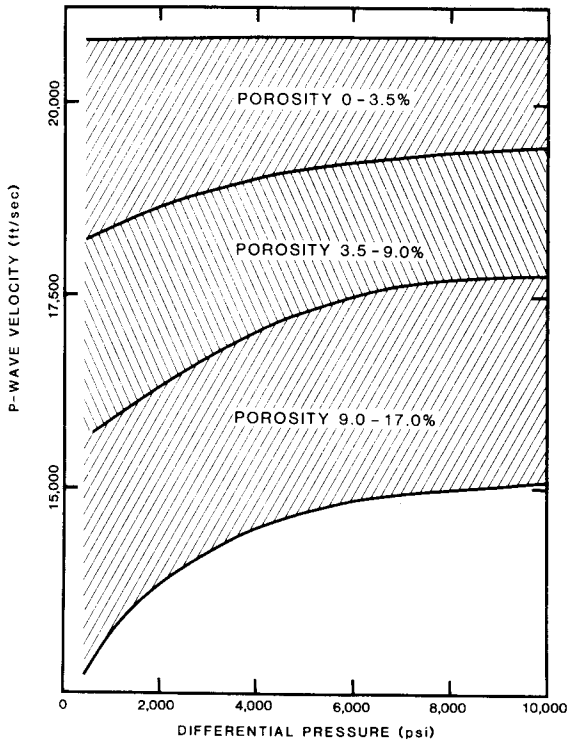

FIG. 7. *P*-wave velocity versus differential pressure for brine-saturated samples (limestone).

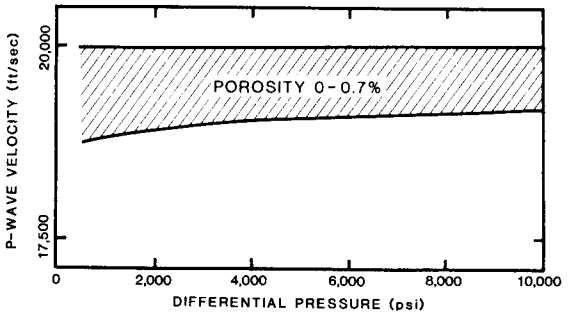

FIG. 9. *P*-wave velocity versus differential pressure for brine-saturated samples (anhydrite).

$$\begin{aligned}\mathrm{VPB} = {} & A_0 + A_1\mathrm{ROB} - A_2\,\mathrm{PHI} - A_3\,\mathrm{QUC} - A_4\,\mathrm{ANC} \\ & - A_5\,\mathrm{CAX} - A_6\,\mathrm{SKG} + A_7(\mathrm{GTO} + \mathrm{CAM}) \\ & - A_8(\mathrm{XTO} + \mathrm{DOX} + \mathrm{DOC} - \mathrm{CAC}),\end{aligned}$$

$$\begin{aligned}\mathrm{VPA} = {} & A_0 + A_1\mathrm{ROA} - A_2\,\mathrm{PHI} - A_3\,\mathrm{QUC} - A_4\,\mathrm{ANC} \\ & - A_5\,\mathrm{CAX} - A_6\,\mathrm{SKG} + A_7(\mathrm{GTO} + \mathrm{CAM}) \\ & - A_8(\mathrm{XTO} + \mathrm{DOX} + \mathrm{DOC} - \mathrm{CAC}),\end{aligned}$$

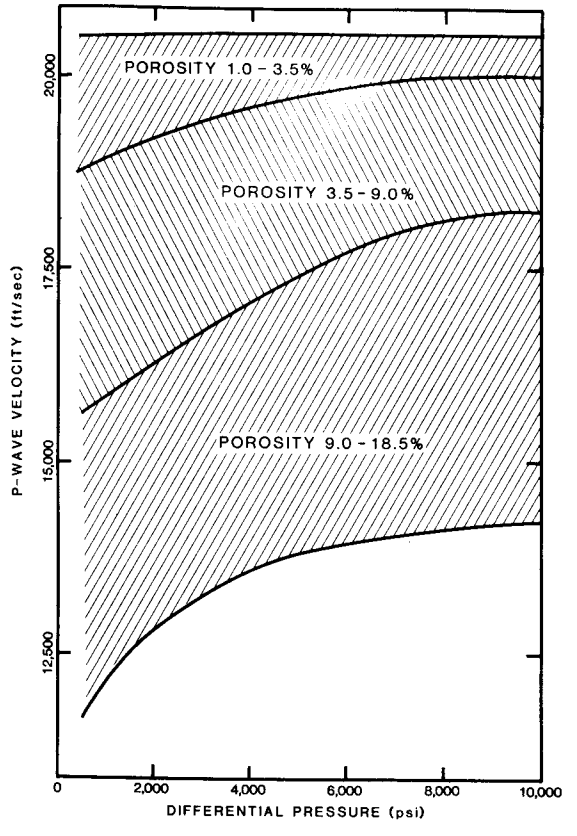

FIG. 8. *P*-wave velocity versus differential pressure for brine-saturated samples (dolomite).

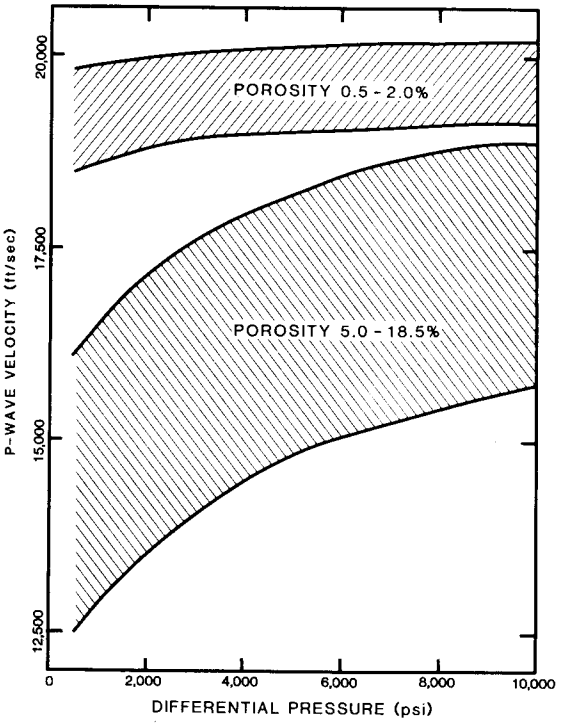

FIG. 10. *P*-wave velocity versus differential pressure for brine-saturated samples (limestone and dolomite).

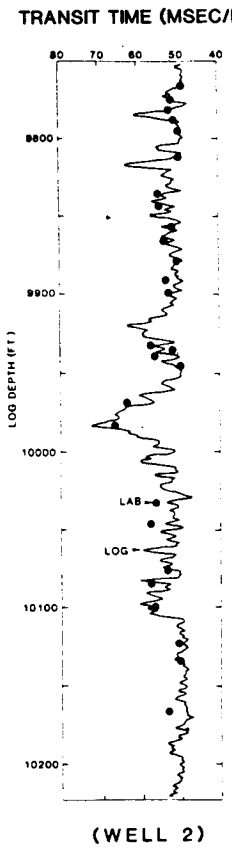

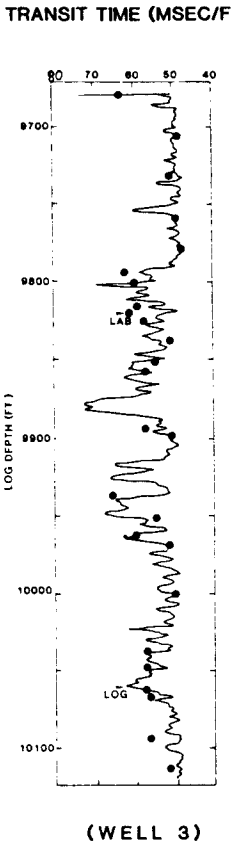

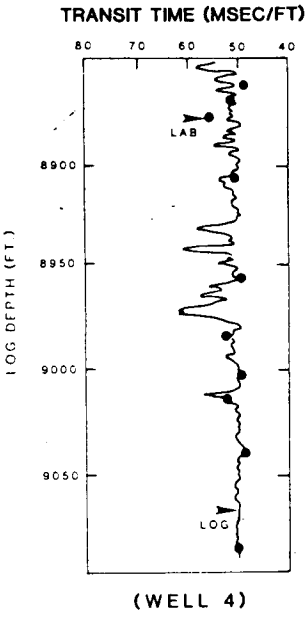

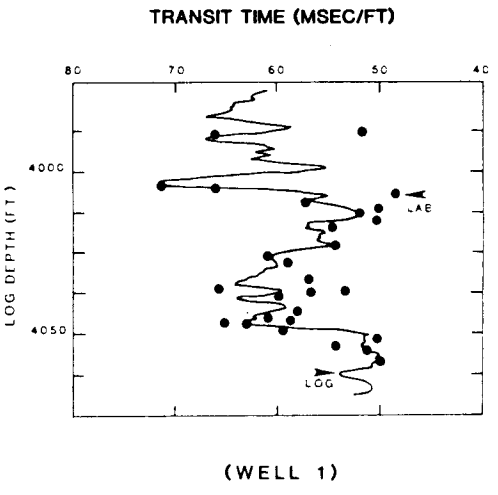

FIG. 11. Comparison of lab *P*-wave transit time with log interval transit time.

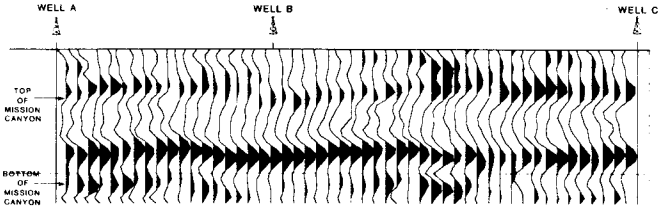

FIG. 12. Seismic window encompassing the Mission Canyon formation from a seismic section of the Little Knife field, Williston basin.

$$\mathrm{VSB} = A_0 + A_1\mathrm{ROB} - A_2\,\mathrm{PHI} - A_3\,\mathrm{QUC} - A_4\,\mathrm{ANC} - A_5\,\mathrm{CAX} - A_6\,\mathrm{SKG} + A_7(\mathrm{GTO} + \mathrm{CAM}) - A_8(\mathrm{XTO} + \mathrm{DOX} + \mathrm{DOC} - \mathrm{CAC}),$$

and

$$\mathrm{VSA} = A_0 + A_1\mathrm{ROA} - A_2\,\mathrm{PHI} - A_3\,\mathrm{QUC} - A_4\,\mathrm{ANC} - A_5\,\mathrm{CAX} - A_6\,\mathrm{SKG} + A_7(\mathrm{GTO} + \mathrm{CAM}) - A_8(\mathrm{XTO} + \mathrm{DOX} + \mathrm{DOC} - \mathrm{CAC}).$$

Coefficients for the independent variables at the differential pressures under which measurements were made are given in Table 4. These data show that the major factors influencing velocities are porosity and bulk density. An increase in porosity decreases velocity; an increase in bulk density increases velocity. An increase in the quartz content decreases velocity but has less influence than porosity. The influence of calcite and dolomite on velocity is variable and smaller than the influence of the first three variables. All other petrographic variables in Table 2 have no significant effect on velocity.

The influence of differential pressure on V_p for brine-saturated rock samples is shown in Figures 7–10 for some of the lithologic groups separated according to Figure 2. A comparison of these plots indicates that the velocity variation with pressure (i.e., the shape of the velocity-pressure curves) is similar for the different lithologic groups when porosity is held constant. We conclude that the pressure effect on velocity is essentially independent of lithology for the samples represented here.

As an extension of this study, the velocity changes associated with the varying content of clay, quartz, and anhydrite in carbonate rocks are investigated.

LABORATORY VERSUS LOG COMPARISON

The laboratory *P*-wave transit time values for the brine-saturated rock samples were superposed at their corresponding depths on the sonic well logs (Figure 11). Despite the fact that sonic logs show the effects of thin beds, caving, mud compositions, and frequency of the signal, we found no systematic shift between lab and log values. The average relative deviation of lab values from log values is not more than ~5 percent. This implies that the laboratory data are representative of the in-situ acoustic data. However, samples with large deviations to the high- or low-velocity side of the log values fall to the high and low sides, respectively, of sharp features on the log. Apparently, the log value is not representative, in such cases, of the high or low velocity of the thin bed from which the lab sample was collected. Consequently, larger deviations between lab and log measurements are caused by inadequate resolution of fine layers by the logging tool.

We conclude that laboratory measurements of *P*-wave velocity for brine-saturated rocks, at simulated in-situ conditions, match well with log acoustic properties.

APPLICATION OF ROCK PROPERTY RESULTS TO THE INTERPRETATION OF A MISSION CANYON *P*-WAVE IMPEDANCE MODEL

Use of an acoustic impedance computed from high-resolution reflection seismic data is a well-established tool in

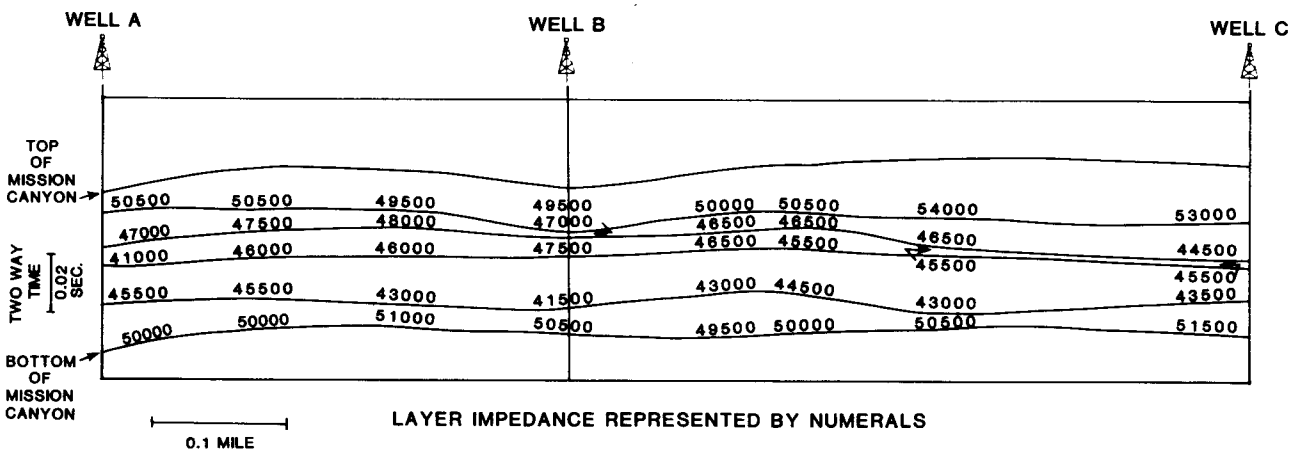

FIG. 13. Stratigraphic model generated by an inverse modeling program.

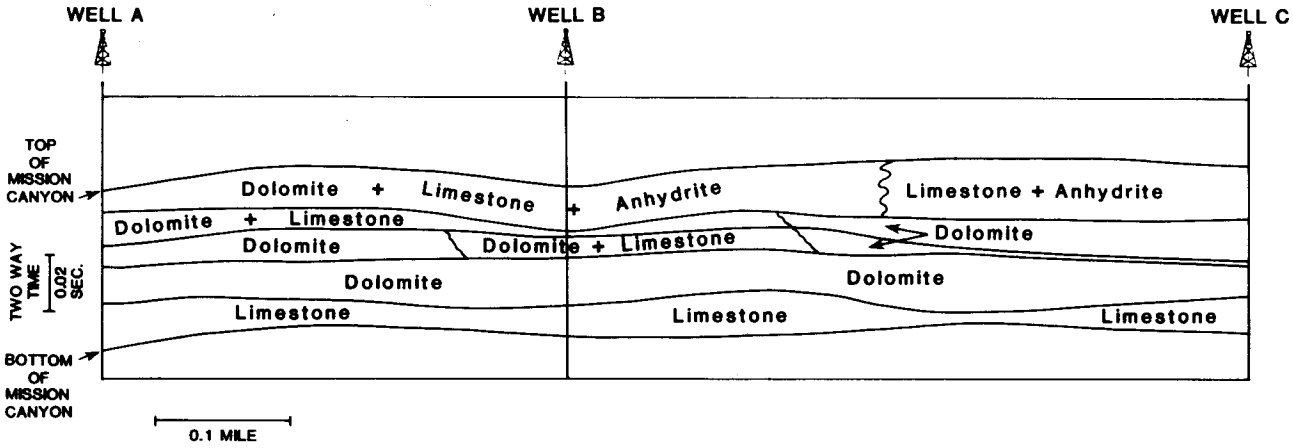

FIG. 14. The lithologic interpreted impedance cross-section.

seismic interpretation (Berteussen and Ursin, 1983). The application of the method on field data was shown by Lavergne and Willm (1977), Lindseth (1979), and Becquey et al. (1979).

We used the rock-property results to interpret a layered *P*-wave impedance model derived from the seismic section (Figure 12). The impedance model was determined using an inversion scheme in which the difference between the amplitudes of the seismic traces and those for synthetic traces (made from an estimated impedance model) were iteratively minimized in terms of impedance and layer thickness using a least-squares criterion. The time window of the seismic data used in the modeling procedure corresponds in the section to the Mission Canyon formation, within the Little Knife field, Williston basin, North Dakota. On the cross-section in Figure 13, the Mission Canyon formation has been subdivided into five layers, within which acoustic impedance values were computed at regular intervals. Our purpose was to translate impedance values into porosities and associate them with lithologies.

LITHOLOGIC INTERPRETATION

Lithologic interpretation of the seismic section using the impedance model, in many respects, depends upon the correct model and accuracy of the impedance values. We don't discuss the problem here, but these factors can be critical and should be considered before applying the technique which we describe below.

The arithmetic means and standard deviations of impedance values calculated for seven rock types (Figure 2), based on 92 samples, are shown in Table 5. Also given is the number of samples used for each lithologic category. Four categories have deficient sample size. This is explained by the fact that dominant lithologies in Mission Canyon cores are limestones and dolomites. Three categories of impedance magnitudes are distinguishable in Table 5. They are limestone, dolomite, and a mixture of limestone and dolomite.

Assuming a normal distribution of impedance values in each group, a most likely assignment approach may be used to classify the seismic impedance values displayed in Figure 13 into specific lithologic categories. An impedance value is assigned to a lithologic category on the basis of the smallest difference from a mean value.

This approach to the discrimination of the different Mission Canyon facies was attempted because the low-porosity anhydrites have impedances systematically greater than limestones which in turn have impedances systematically greater than the high-porosity dolomites. This discrimination, which uses only *P*-wave data, cannot be expected to work in general. Note, however, that if *S*-wave seismic data were also available, a discrimination of carbonate rock types could be made in many cases using the data in Figure 4.

The interpreted impedance cross-section is shown in Figure 14. According to Table 5 the top and bottom layers correspond to intermediate impedance values which could be either limestone or combinations of anhydrite, limestone, and dolomite. Using regional well data for this area (Figure 15), we established that the upper layer should be interpreted as a combination of anhydrite, limestone, and dolomite, while the bottom layer should be interpreted as a low-porosity limestone. According to our lithologic groups the three intermediate layers have lower impedance values and are interpreted as dolomites and combinations of limestones and dolomites. These results match the lithologic interpretation derived from well data (Figure 15).

Table 5. Arithmetic means and standard deviations of impedance values for the seven lithologic types (*N* is the number of samples in a group).

Lithologic type	Mean	Standard deviation	*N*
1 (Ca)	50 700	4 400	29
2 (Ca-An)	54 900		1
3 (An)	57 500	1 200	4
4 (An-Do)	57 400	3 200	2
5 (Do)	45 700	5 600	30
6 (Ca-Do)	47 000	5 800	21
7 (An-Ca-Do)	50 300	7 000	5

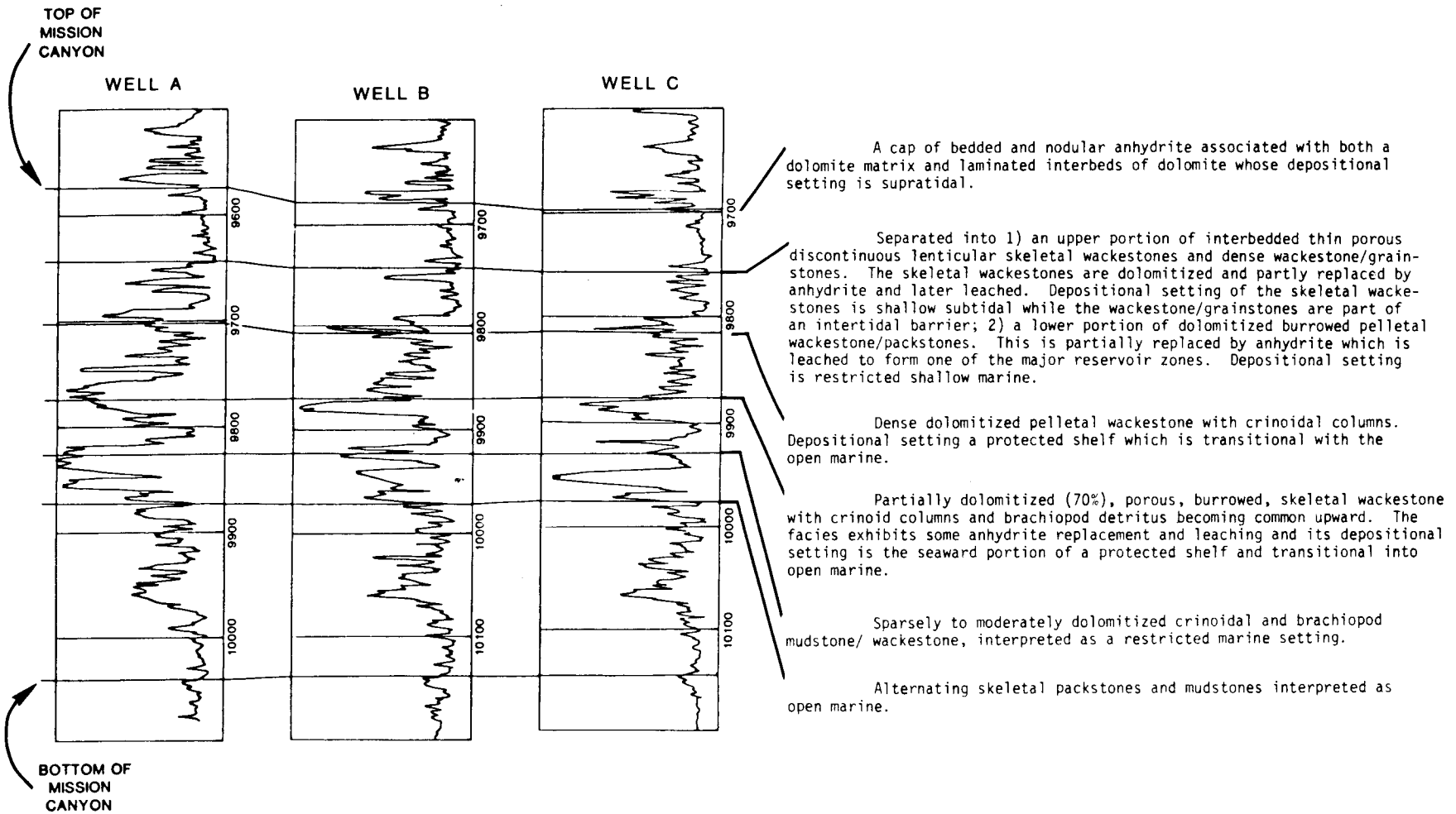

FIG. 15. Sonic logs of wells shown in cross-section of Figure 14.

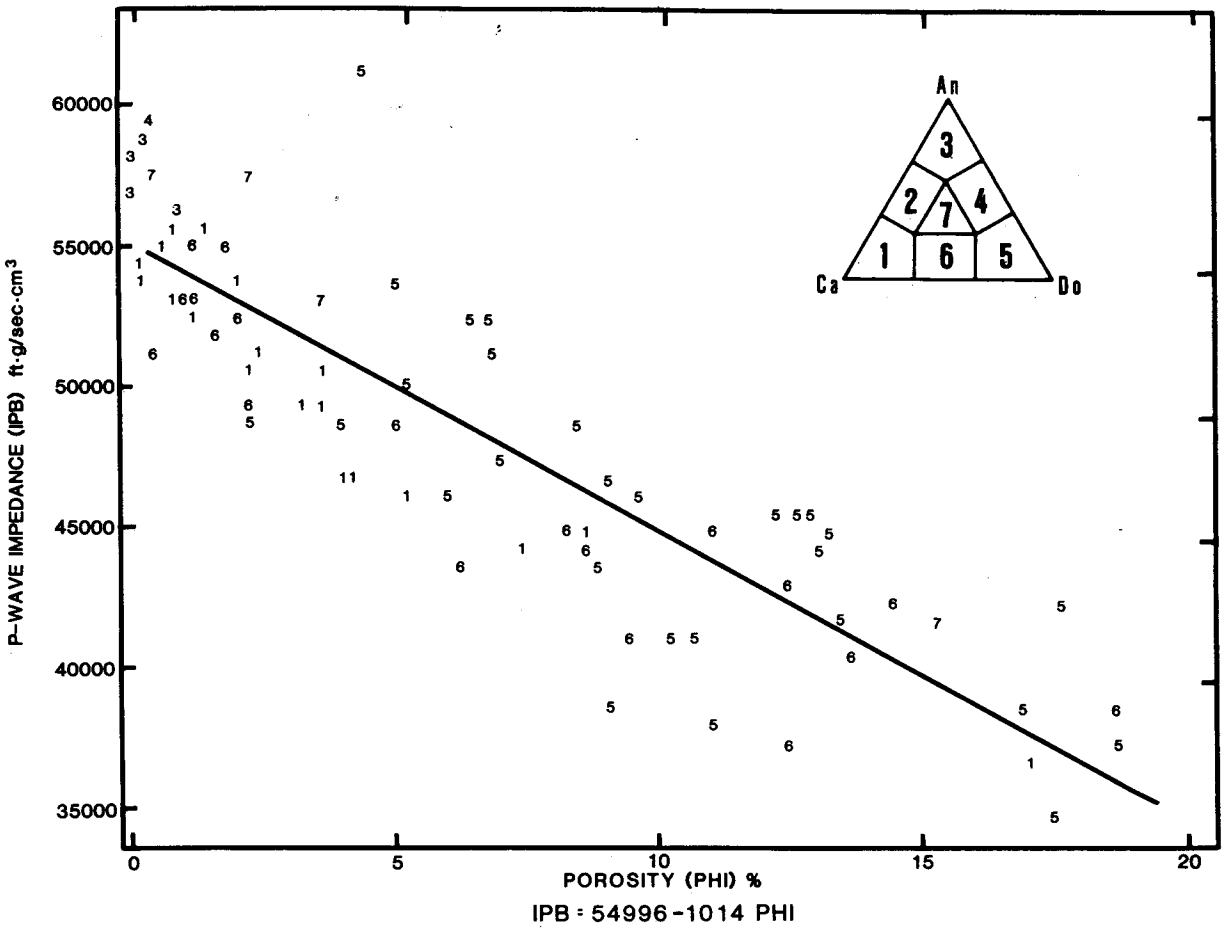

FIG. 16. Plot of *P*-wave impedance versus porosity for brine-saturated samples.

Table 6. Comparison of porosities derived from sonic log using the time-average equation with those derived from inverse model using porosity curve of Figure 16.

Well		Sonic log porosity (percent)	Model	
			Impedance	Porosity (percent)
A	Non-porous zone 9 575–9 645 ft on the log 9 875–10 040 ft on the log	0	50 500 50 000	4–5 4.5–5.5
	Porous zone 9 645–9 875 ft on the log	2–15	47 000 41 000	7.5–8.5 13.5–14.5
B	Non-porous zone 9 680–9 740 ft on the log 9 970–10 140 ft on the log	0	49 500 50 500	5–6 4–5
	Porous zone 9 740–9 970 ft on the log	6–15	47 500 41 500	6.5–7.5 12.5–13.5
C	Non-porous zone 9 700–9 760 ft on the log 9 975–10 140 ft on the log	0	53 000 51 500	2.5–3.5 3–4
	Porous zone 9 760–9 975 ft on the log	7 12	45 500 43 500	9–10 10.5–11.5

ESTIMATION OF POROSITY

Porosities in the Mission Canyon layers were estimated by translating the impedance values into porosity values using the means of the impedance-porosity regression curve of Figure 16. The impedance cross-section in Figure 14 intersects three wells (Figure 15). These values were compared (in Table 6) with the porosity values calculated from the sonic logs using the time-average equation. There is good agreement between porosities derived from the sonic logs and those determined from the inverted seismic section. We conclude that the method for evaluating porosity variations works well in the Mission Canyon case.

CONCLUSIONS

(1) The major factors influencing velocity are porosity and bulk density. An increase in porosity decreases velocity; an increase in bulk density increases velocity. An increase in the quartz content decreases velocity but has less influence than porosity. The influence of calcite and dolomite on velocity is variable and smaller than the influence of the first three variables. The influences of all other variables in this data set, including pore fluid, are not statistically significant.

(2) The velocity ratio V_p/V_s can be used to discriminate between limestones and dolomites.

(3) When the appropriate matrix velocities are used, the time-average curves show a good correspondence to the laboratory data and so can be used to estimate porosity quite accurately.

(4) Laboratory measurements of V_p for brine-saturated rocks at simulated in-situ conditions reliably reproduce well-log acoustic properties.

(5) The results of a rock-property study can be used to interpret impedance cross-sections generated by a seismic inversion process. In studying the Mission Canyon cross-section from the Williston basin, we found that our interpreted lithologies and porosities are consistent, in most cases, with an accepted interpretation derived from well logs.

ACKNOWLEDGMENTS

The authors wish to thank J. G. Towle for the laboratory measurements he made, C. G. Abry and G. J. Stauffer for helping with our analysis, and the Gulf Research and Development Company for encouraging publication of the results of our research.

REFERENCES

Becquey, M., Lavergne, M., and Willm, C., 1979, Acoustic impedance logs computed from seismic traces: Geophysics, **44**, 1485–1501.
Benzing, W. M., 1978, V_s/V_p relationships in carbonates and sandstones: laboratory data: Presented at the 48th Annual International SEG Meeting, San Francisco.
Berteussen, A. K., and Ursin, B., 1983, Approximate computation of the acoustic impedance from seismic data: Geophysics, **48**, 1351–1358.
Birch, F., 1960, The velocity of compressional waves in rocks to 10 kilobars, Part 1: J. Geophys. Res., **65**, 1083–1102.
Bryant, C. E., 1960, Statistical analysis: McGraw-Hill Book Co., Inc., 198–224.
Domenico, S. N., 1976, Effect of brine-gas mixture on velocity in an unconsolidated sand reservoir: Geophysics, **41**, 882–894.
Eastwood, L. R., 1983, Basis for interpretation of V_p/V_s ratios in complex lithologies: Soc. Prof. Well Log Analysts 24th Annual Logging Symp. G1-G17.
Gardner, G. H. F., and Harris, M. H., 1968, Velocity and attenuation of elastic waves in sand: Soc. Prof. Well Log Analysts 9th Annual Logging Symp., M1–M19.
Gassman, F., 1951, Über die Elastizität Poröser Medien: Vierteljahrsscr. Naturforsch. Ges., **96**, Part B, 1–23.
Gregory, A. R., 1976, Fluid saturation effects on dynamic elastic properties of sedimentary rocks: Geophysics, **41**, 895–921.
——— 1977, Aspects of rock physics from laboratory and log data that are important to seismic interpretation: Am. Assoc. Petr. Geol. Memoir 26, 15–46.
Harman, H. H., 1976, Modern factor analysis: 3rd ed., revised: Univ. of Chicago Press, 487.
Hashin, Z., and Shtrikman S., 1962, A variational approach to the theory of the elastic behavior of polycrystals: J. Mech. and Phys. Solids, **10**, 343–352.
Hill, R., 1952, The elastic behavior of a crystalline aggregate: Proc. Phys. Soc. London (A), **65**, 349–354.
Johnson, W. E., 1978, Relationship between shear-wave velocity and geotechnical parameters: Presented at the 48th Annual International SEG Meeting, San Francisco.
King, M. S., 1966, Wave velocities in rocks as a function of changes in overburden pressure and pore fluid saturans: Geophysics, **31**, 50–73.
Kithas, B. A., 1976, Lithology, gas detection, and rock properties from acoustic logging systems: Soc. Prof. Well Log Analysts 17th Ann. Logging Symp., R1–R10.
Kuster, G. T., and Toksöz, M. N., 1974a, Velocity and attenuation of seismic waves in two-phase media: Part 1. Theoretical formulation: Geophysics, **39**, 587–606.
——— 1974b, Velocity and attenuation of seismic waves in two-phase media: Part II—Experimental results: Geophysics, **39**, 607–618.
Lavergne, M., and Willm, C., 1977, Inversion of seismograms and pseudo velocity logs: Geophys. Prosp., **25**, 231–250.
Lindseth, R. O., 1979, Synthetic sonic logs—A process for stratigraphic interpretation: Geophysics, **44**, 3–26.
Nations, J. F., 1974, Lithology and porosity from acoustic shear and compressional wave transit-time relationships: Soc. Prof. Well Log Analysts 15th Ann. Logging Symp., Q1–Q16.
Pickett, G. R., 1963, Acoustic character logs and their application in formation evaluation: J. Petr. Tech., 659–667.
Reuss, A., 1929, Berechnung der Fliessgrenze von Mischkristallen auf Grund der Plastizitätsbedingung für Einkristalle: Z. Angew. Math. Mech., **9**, 49–58.
Tatham, R. H., and Stoffa, P. L., 1976, V_p/V_s—A potential hydrocarbon indicator: Geophysics, **41**, 837–849.
Tatham, R. H., 1982, V_p/V_s and lithology: Geophysics, **47**, 336–344.
Voigt, W., 1928, Lehrbuch der Krystallphysik: B. G. Teubner, 962.